Journal of the Eastern Asia Society for Transportation Studies, Vol. 6, pp. 1231 - 1246, 2005

SIMULATION OF GEOSYNTHETIC-REINFORCED PLANE STRAIN COMPRESSION (PSC) TEST OF TOYOURA SAND

Mohammed S. A. SIDDIQUEE
Professor
Civil Engineering Department, Bangladesh University of Engineering & Technology, (BUET), Dhaka-1000, Bangladesh
Fax: +88-02-8613026
E-mail: sid@ce.buet.ac.bd

Eqramul Hoque
Associate Professor
Civil Engineering Department, Bangladesh University of Engineering & Technology, (BUET), Dhaka-1000, Bangladesh
Fax: +88-02-8613026
E-mail: ehoq@ce.buet.ac.bd

Warat KONGKITKUL
JSPS Fellow
Graduate School of Engineering
Tokyo University of Science,
Noda-shi, Chiba,
Japan
FAX: 03-5841-8504
E-mail: warat@rs.noda.tus.ac.jp

Fumio TATSUOKA
Professor,
Department of Civil Engineering
Tokyo University of Science
Noda-shi, Chiba,
Japan
FAX: 03-5841-8504
E-mail: tatsuoka@rs.noda.tus.ac.jp

Abstract: A stress-strain model called TESRA (Temporary Effects of Strain Rate and Acceleration) , described in a non-linear three-component framework, has been developed to simulate the viscous effects on the stress-strain behaviour observed in an extensive series of drained plane strain compression (PSC) tests on clean sands. A similar model has been developed for the geosynthetic reinforcement also. The TESRA model was implemented into a generalized elasto-plastic isotropic strain-hardening nonlinear Finite Element code. The integration scheme to obtain the viscous and inviscid stress components according to the TESRA model in FEM analysis, which needs some specific considerations including the relevant choice of the suitable rate parameter, is described. The geosynthetic reinforcements were modelled by employing nonlinear elasto-plastic one-dimensional truss elements with three-component TESRA model. The axial force – axial strain – time relations of several types of geosynthetic reinforcements were successfully simulated by the present FE code called - "Geotechnical Nonlinear Analysis (GNA)".The shear stress – shear (or axial) strain - time relations from two drained PSC tests on geosynthetic reinforced Toyoura sand were successfully simulated by the FE code embedded with the TESRA model. It is shown that the FE code can predict the time-dependent stress-strain behaviour of reinforced sand accurately without spending any significant extra computational time or storage.

Key Words: FEM simulation, Loading rate effect, Plane strain compression tests, Geosynthetic reinforcement, Viscous property of sand.

1. INTRODUCTION

Kotake et al. (1999) and Villard et al. (2002) performed FEM analysis of the results obtained by performing drained PSC tests on Toyoura sand reinforced with one layer of various kinds of reinforcement (Tatsuoka and Yamaguchi, 1986 as well as the unreinforced ones. They found that the failure of reinforced sand can be reasonably simulated only by a non-linear elasto-plastic FEM which properly takes into account strain localisation as well as the intrinsic

strength and deformation characteristics of sand and interface properties. Hirakawa et al. (1998) performed large-size PSC tests on unreinforced and reinforced dense Toyoura sand. In these tests, effects of the total tensile rigidity per reinforcement layer and the covering ratio of each reinforcement layer were investigated systematically by using: a) a set of different grids having different total tensile rigidities with the same covering ratio; and b) another set of different grids having different covering ratios with the same total tensile rigidities. That is, the specimens were reinforced with the PVA geogrid layers reconstructed to have different structures with different rigidities and covering ratios. The results obtained from large-size PSC tests were simulated by plane strain non-linear elasto-plastic FEM considering strain localisation, anisotropic stress-strain properties of sand and interface properties (Peng et al., 2000). However, any effect of material viscous properties was not taken into account in the above-mentioned FEM analysis.

The loading rate effects due to material viscosity on the stress-strain behavior of sand (not due to delayed dissipation of excess pore water) are often very important in Geotechnical Engineering practice. A number of researchers (e.g., Murayama et al., 1984; Di Benedetto & Tatsuoka, 1997; Lade & Liu, 1998; Matsushita et al., 1999; Di Benedetto et al. 2002; Tatsuoka et al. 2002; Kuwano & Jardine, 2002; Nawir et al., 2003a, b; Tatsuoka, 2004) reported significant loading rate effects observed in laboratory stress-strain tests on sand; i.e., effects of strain rate and its change on the stress-strain relation, creep deformation and stress-relaxation during otherwise monotonic loading (ML) at a constant strain rate.

Within the framework of the general non-linear three-component model (Fig. 1), Di Benedetto et al. (2002) and Tatsuoka et al. (2002) proposed a set of stress-strain models to simulate the effects of material viscosity on the stress-strain behaviour of geomaterial (i.e., clay, sand, gravel and softrock) and geosynthetic reinforcements. They showed that the viscous property of clean sand (i.e., uniform sand) is different from that of clay or geosynthetics in that the viscous effect decays with an increase in the irreversible strain and proposed a specific model to describe the above (i.e., the TESRA model explained below). In this paper, it is shown that this model can be smoothly implemented in a FE code. Then, axial force – axial strain relations of geosynthetic reinforcements and shear stress – shear (or axial) strain relations from typical drained geosynthetic reinforced plane strain compression (PSC) tests on clean sands (Toyoura sands) were simulated by the FE code embedded with the TESRA model.

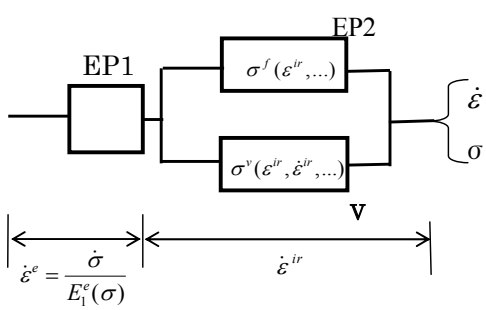

Fig. 1 General non-linear non-linear three-component model (Di Benedetto, 1987).

In this paper, viscous effects on the relationship between the shear stress and the shear strain or the axial strain, which is always approximately proportional to the shear strain, in drained PSC at fixed confining pressure are discussed and analysed.

2. MODEL DESCRIPTION

The non-linear three component model, depicted in Fig. 1, has the following general features:

1) A given total strain rate, $\dot{\varepsilon}$, is decomposed into the elastic component, $\dot{\varepsilon}^e$, and the irreversible (or inelastic or visco-plastic) component, $\dot{\varepsilon}^{ir}$ (or $\dot{\varepsilon}^{vp}$). Di Benedetto et al. (2002) assumed that $\dot{\varepsilon}^e$ takes place only in component *EP1*, while component *EP2* exhibits $\dot{\varepsilon}^{ir}$ only. This assumption greatly simplifies the model parameter determination, while it does not sacrifice the accuracy of simulation when sufficiently small increments are used. ε^e is obtained by integrating for a given stress path as $\varepsilon^e = \int d\varepsilon^e$, where $d\varepsilon^e = d\sigma / E^e(\sigma)$; where $E^e(\sigma)$ is the tangent elastic stiffness, which is a function of instantaneous stress σ (and others) (i.e., the hypo-(quasi)-elastic model; Tatsuoka & Kohata, 1995; Hoque & Tatsuoka, 1998; Tatsuoka et al., 1999a, b).
2) The total component of a given effective stress, σ, which is herein called the total stress component, is decomposed into the time-independent (inviscid) and time-dependent (viscous) components, σ^f and σ^v, as:

$$\sigma = \sigma^f\left(\varepsilon^{ir}, h_s\right) + \sigma^v \tag{1a}$$

where $\sigma^f\left(\varepsilon^{ir}, h_s\right)$ means the σ^f - ε^{ir} relation, called the reference stress-strain relation, whatever strain (or stress) rates take place when traveling along a given strain (ε^{ir}) or stress (σ^f) path (with or without cyclic loading); and h_s is the parameter representing the loading history. Different σ^f - ε^{ir} relations are therefore formed for loading, unloading, reloading and so on. Empirical σ^f - ε^{ir} relations obtained for respective test conditions were used in the present study. σ^v is the viscous stress component, which is a function of ε^{ir} and its rate, $\dot{\varepsilon}^{ir} = \partial\dot{\varepsilon}^{ir} / \partial t$, and the history parameter.

For primary ML in which the irreversible strain rate, $\dot{\varepsilon}^{ir}$, is always positive, the history parameter h_s for σ^f in Eq. 1a becomes unnecessary and Eq. 1a is rewritten as:

$$\sigma = \sigma^f\left(\varepsilon^{ir}\right) + \sigma^v \tag{1b}$$

Di Benedetto et al. (2002) and Tatsuoka et al. (2002) showed that at least three different functional forms of the viscous component, σ^v, are necessary to describe the different viscous properties of geomaterial. Firstly, a stress-strain model called the "new isotach" was proposed to describe the loading rate effects of clay-like materials, for which, for primary ML, the current value of σ^v is a non-linear function of instantaneous value of $\dot{\varepsilon}^{ir}$ while it is always proportional to the instantaneous value of σ^f as:

$$\sigma^v\left(\varepsilon^{ir}, \dot{\varepsilon}^{ir}\right) = \sigma^f\left(\varepsilon^{ir}\right) \cdot g_v(\dot{\varepsilon}^{ir}) \tag{2}$$

$$\sigma = \sigma^f\left(\varepsilon^{ir}\right) \cdot \{1 + g_v(\dot{\varepsilon}^{ir})\} \tag{3}$$

where $g_v(\dot{\varepsilon}^{ir})$ is the viscosity function, which is always zero or positive and given as follows for any strain (ε^{ir}) or stress (σ^f) path (with or without cyclic loading):

$$g_v(\dot{\varepsilon}^{ir}) = \alpha \cdot [1 - \exp\{1 - (\frac{\left|\dot{\varepsilon}^{ir}\right|}{\dot{\varepsilon}_r^{ir}} + 1)^m\}] \quad (\geq 0) \tag{4}$$

where $\left|\dot{\varepsilon}^{ir}\right|$ is the absolute value of $\dot{\varepsilon}^{ir}$; and α, $\dot{\varepsilon}_r^{ir}$ and m are positive material constants. According to this model, as far as ML continues, the viscous stress component, σ^v, is a unique function of instantaneous values of ε^{ir} and $\dot{\varepsilon}^{ir}$, independent of previous loading history. The term "new" of the model name comes from that, with the original isotach model (Suklje, 1966), the stress σ (therefore σ^v) is a function of instantaneous strain rate, $\dot{\varepsilon} = \partial\dot{\varepsilon} / \partial t$, not $\dot{\varepsilon}^{ir}$, while, with the new isotach model, σ^v is a function of $\dot{\varepsilon}^{ir}$. This

difference results into significant differences in the model behaviour, in particular during stress relaxation with $\dot{\varepsilon} = 0$ and immediately after a step change in $\dot{\varepsilon}$ during otherwise ML at a constant $\dot{\varepsilon}$ (Tatsuoka et al., 1999a).

Then, Di Benedetto et al. (2002) and Tatsuoka et al. (2002) modified the new isotach model so that such a decay of viscous effect with an increase in ε^{ir} as described above can be properly described by revising Eq. 2 as follows:

$$\begin{aligned}\sigma^{v} &= \int_{\tau=\varepsilon_1^{ir}}^{\varepsilon^{ir}} \left[d\sigma^{v}\right]_{(\tau,\varepsilon^{ir})} = \int_{\tau=\varepsilon_1^{ir}}^{\varepsilon^{ir}} \left[d\sigma^{v}\right]_{(\tau)} \cdot g_{decay}(\varepsilon^{ir}-\tau) \\ &= \int_{\tau=\varepsilon_1^{ir}}^{\varepsilon^{ir}} \left[d\{\sigma^{f} \cdot g_{v}(\dot{\varepsilon}^{ir})\}\right]_{(\tau)} \cdot g_{decay}(\varepsilon^{ir}-\tau)\end{aligned} \tag{5}$$

where σ^{v} is the current viscous stress component (when $\varepsilon^{ir} = \varepsilon^{ir}$); and the term $\left[d\sigma^{v}\right]_{(\tau,\varepsilon^{ir})}$ is the viscous stress increment that developed in the past when $\varepsilon^{ir} = \tau$ and has decayed until the present (when $\varepsilon^{ir} = \varepsilon^{ir}$). The term $\left[d\sigma^{v}\right]_{(\tau,\varepsilon^{ir})}$ is therefore represented by the term, $\left[d\sigma^{v}\right]_{(\tau)} \cdot g_{decay}(\varepsilon^{ir}-\tau)$, where $\left[d\sigma^{v}\right]_{(\tau)}$ is the viscous stress increment that developed following Eq. 2 when $\varepsilon^{ir} = \tau$, equal to $\left[d(\sigma^{f} \cdot g_{v}(\dot{\varepsilon}^{ir})\right]_{(\tau)}$; ε_1^{ir} is the strain at the start of integration, where $\sigma^{v} = 0$; and $g_{decay}(\varepsilon^{ir}-\tau)$ is the decay function, given as follows (Tatsuoka et al. 2000; Di Benedetto et al., 2002) :

$$g_{decay}(\varepsilon^{ir}-\tau) = r_1^{(\varepsilon^{ir}-\tau)} \tag{6a}$$

where r_1 is a positive constant smaller than unity. Although other forms that are different from the power form of Eq. 6a can describe the decay of σ^{v} with an increase in ε^{ir}, the available experimental results support this form of equation, while the power form has a fundamental advantage over than the other forms as described later in this paper (Di Benedetto et al., 2002). The physical meaning of the decay parameter r_1 of the decay function (Eq. 6a) can be readily seen by rewriting to:

$$g_{decay} = (0.5)^{\frac{\varepsilon^{ir}-\tau}{H}} \tag{6b}$$

where H is the irreversible strain increment, $\varepsilon^{ir} - \tau$, by which the viscous stress increment $[d\sigma^{v}]_{(\tau)}$ becomes a half as ML continues. The relationship between the parameters r_1 and H is given by:

$$r_1 = \left(\frac{1}{2}\right)^{\frac{1}{H}}; \text{ or } H = \frac{\log(1/2)}{\log(r_1)} \tag{6c}$$

H decreases with a decrease in r_1. When $r_1 = 1.0$, H becomes infinitive. On the other hand, when $r_1 = 0$, H becomes zero.

When $r_1 = 1.0$, the integration of Eq. 5 becomes totally differential and Eq. 5 returns to Eq. 2 (the new isotach model). By this decay feature (Eqs. 6a & 6b), the effects of irreversible strain rate, $\dot{\varepsilon}^{ir} = \partial\varepsilon^{ir}/\partial t$, and its rate (i.e., irreversible strain acceleration) , $\ddot{\varepsilon}^{ir} = \partial^2\varepsilon^{ir}/\partial t^2$, on σ^{v} becomes non-persistent, or temporary, during subsequent ML at a constant $\dot{\varepsilon}^{ir}$. The new model is called the TESRA model according to this property (i.e., **t**emporary **e**ffects of irreversible **s**train rate and irreversible **s**train **a**cceleration on the viscous stress component). As demonstrated by Di Benedetto et al. (2002) and Tatsuoka et al. (2002), when r_1 is less than unity, the value of σ^{v} could become either positive or zero or negative depending on recent loading history even when $\dot{\varepsilon}^{ir}$ has been kept positive. The procedure to obtain the model parameters is explained in Di Benedetto et al. (2002).

In the present study, the TESRA model was implemented into an existing non-linear elasto-plastic FE code (Siddiquee et al., 1999, 2001a, b). Some specific considerations were made on the relevant choice of the internal variable for loading rates, which is the key for the success of this implementation. The FE code enriched with the TESRA model were validated by simulating the shear stress – shear (or axial) strain relations from drained PSC tests on sand and axial force – axial strain of geosynthetic reinforcement, showing that this FE code can predict the viscous effects on the stress-strain behaviour of reinforced sand quite accurately without spending any significant extra computational time or storage.

3. IMPLEMENTATION OF 'TESRA' MODEL INTO A FE CODE

3.1 Formulation of TESRA model

Eq. 2 can be rewritten as:

$$\sigma^{v} = \int_{\tau=\varepsilon_1^{ir}}^{\varepsilon^{ir}} \left[\left(\frac{\partial \sigma^{f}}{\partial \varepsilon^{ir}} \right) \cdot g_{v}(\dot{\varepsilon}^{ir}) + \sigma^{f} \cdot \left(\frac{\partial g_{v}(\dot{\varepsilon}^{ir})}{\partial \dot{\varepsilon}^{ir}} \right) \cdot \frac{\ddot{\varepsilon}^{ir}}{\dot{\varepsilon}^{ir}} \right]_{(\tau)} \cdot d\tau \tag{7}$$

where the term $[(\partial\sigma^{f}/\partial\varepsilon^{ir})\cdot g_{v}(\dot{\varepsilon}^{ir})\cdot d\varepsilon^{ir}]_{(\tau)}$ represents the component of $[d\sigma^{v}]_{(\tau)}$ that develops by $d\varepsilon^{ir}$ when $\varepsilon^{ir}=\tau$ during ML at a constant $\dot{\varepsilon}^{ir}$ (i.e., the effect of irreversible strain rate); and the second term $[\sigma^{f}\cdot(\partial g_{v}(\dot{\varepsilon}^{ir})/\partial\dot{\varepsilon}^{ir})\cdot d\dot{\varepsilon}^{ir}]_{(\tau)}$ represents the component of $[d\sigma^{v}]_{(\tau)}$ that develops by the increment of irreversible strain rate, $d\dot{\varepsilon}^{ir}$, at a fixed ε^{ir} $(=\tau)$ (i.e., the effect of irreversible strain acceleration). By substituting Eq. 6a into Eq. 5 while referring to Eq. 7, we obtain:

$$\sigma^{v} = \int_{\tau=\varepsilon_1^{ir}}^{\varepsilon^{ir}} \left[\left(\frac{\partial \sigma^{f}}{\partial \varepsilon^{ir}} \right) \cdot g_{v}(\dot{\varepsilon}^{ir}) + \sigma^{f} \cdot \left(\frac{\partial g_{v}(\dot{\varepsilon}^{ir})}{\partial \dot{\varepsilon}^{ir}} \right) \cdot \frac{\ddot{\varepsilon}^{ir}}{\dot{\varepsilon}^{ir}} \right]_{(\tau)} \cdot \eta^{(\varepsilon^{ir}-\tau)} \cdot d\tau \tag{8}$$

When directly using Eq. 8 to obtain the current value of σ^{v}, an integration procedure should be repeated for every small increment of ε^{ir} to update the value of σ^{v}.

On the other hand, an incremental solution technique is usually employed in the FEM. Therefore, it is extremely difficult, if not impossible, to perform to obtain a solution for a given boundary value problem by a FE code in which Eq. 8 is implemented. Tatsuoka et al. (2002) showed that Eq. 8 can be transformed into the following incremental form without losing accuracy for a sufficiently small increment:

$$\begin{aligned}
\sigma^{v} &\cong \int_{\tau=\varepsilon_1^{ir}}^{\varepsilon^{ir}-\Delta\varepsilon^{ir}} \left[d\sigma^{f} \cdot g_{v}(\dot{\varepsilon}^{ir}) \right]_{(\tau)} \cdot g_{decay}(\varepsilon^{ir}-\tau) \cdot d\tau + \Delta\sigma^{v} \\
&= \left[\int_{\tau=\varepsilon_1^{ir}}^{\varepsilon^{ir}-\Delta\varepsilon^{ir}} \left[d\sigma^{f} \cdot g_{v}(\dot{\varepsilon}^{ir}) \right]_{(\tau,h)} \cdot r_1^{(\varepsilon^{ir}-\tau-|\Delta\varepsilon^{ir}|)} \cdot d\tau \right] \cdot r_1^{|\Delta\varepsilon^{ir}|} + \Delta\sigma^{v} \\
&= \left[\sigma^{v} \right]_{(\varepsilon^{ir}-\Delta\varepsilon^{ir})} \cdot r_1^{|\Delta\varepsilon^{ir}|} + \Delta\{\sigma^{f} \cdot g_{v}(\dot{\varepsilon}^{ir})\} \cdot r_1^{\frac{|\Delta\varepsilon^{ir}|}{2}}
\end{aligned} \tag{9}$$

where $\left[\sigma^{v}\right]_{(\varepsilon^{ir}-\Delta\varepsilon^{ir})}$ is the viscous stress at one step immediately before, where the irreversible strain is equal to $\varepsilon^{ir}-\Delta\varepsilon^{ir}$; $\Delta\varepsilon^{ir}$ is the irreversible strain increment taking place between one step immediately before and the current step, which is positive for loading; and $\Delta\{\sigma^{f}\cdot g_{v}(\dot{\varepsilon}^{ir})\}$ is the difference in $\sigma^{f}\cdot g_{v}(\dot{\varepsilon}^{ir})$ between the current step and one step

immediately before, given as:

$$\Delta\{\sigma^f \cdot g_v(\dot{\varepsilon}^{ir})\} = \left[\sigma^f \cdot g_v(\dot{\varepsilon}^{ir})\right]_{[\varepsilon^{ir}]} - \left[\sigma^f \cdot g_v(\dot{\varepsilon}^{ir})\right]_{[\varepsilon^{ir}-\Delta\varepsilon^{ir}]} \tag{10}$$

So, for given values of $\left[\sigma^v\right]_{(\varepsilon^{ir}-\Delta\varepsilon^{ir})}$ as well as the parameters representing the loading history between one step immediately before and the current step (i.e., the values of $\Delta\varepsilon^{ir}$ and Δt or $\dot{\varepsilon}^{ir} = \Delta\varepsilon^{ir} / \Delta t$), the values of ε^{ir} and σ^v at the current state (where $\varepsilon^{ir} = \varepsilon^{ir}$) can be obtained by Eqs. 9 and 10 without repeating the integration from the start of loading. Repeating this incremental procedure from the start of loading, the whole stress-strain-time relation for any given history of strain or stress can be obtained. In the present FEM simulation, a one-step Euler type integration was employed with Eq. 9. This method is very fast despite that the use of Eq. 9 has some restrictions in accuracy and stability.

3.2 Implementation into a FE code

The TESRA model was implemented into an existing nonlinear elasto-plastic FE code (Siddiquee et al., 1999, 2001a,b), which was developed based on the matrix-free dynamic relaxation (DR) technique that was highly optimized for very fast and accurate computation of highly nonlinear equations emerging from material non-linearity. Due to the inherent features of the DR technique, the following steps were revised carefully when implementing the TESRA model into the FE code. Details of the implementation is explained in Ref. (Siddiquee, M. S. A. and Tatsuoka, F. (2001b))

4. NUMERICAL SIMULATION BY FEM

4.1 Material model

The generalized elasto-plastic isotropic strain-hardening and softening model takes into account strain localization associated with shear banding by introducing a characteristic width of shear band in the additive elasto-plastic decomposition of strain. Unlike the method used by Pietruszczak and Mroz (1981), the direction of shear band is not specified in each element, but it is implicitly assumed that, in a given boundary value problem, the direction of shear band coincides with the global direction of local maximum shear strain among adjacent multiple elements. A generalized hyperbolic equation (GHE) (Tatsuoka et al., 1993) is used as the growth function of the yield surface of the generalized Mohr-Coulomb type, given by:

$$\Phi = -\eta I_1 + \frac{1}{g(\theta)}\sqrt{J_2} - K \tag{11}$$

where I_1 is the first stress invariant (i.e., hydrostatic stress component, positive in compression); and J_2 is the second stress invariant (i.e., deviatoric stress). The growth function is explained in details in Siddiquee et al. (1999, 2001a & b). The function $g(\theta)$ in Eq. 11 is the Lode angle function, defined as;

$$g(\theta) = \frac{3 - \sin\phi_{mob}}{2\sqrt{3}\cos\theta - 2\sin\theta\sin\phi_{mob}} \tag{12}$$

In Eq. 11, η is the deviatoric stress at θ=30° (on the π-plane), which is related to the

mobilized angle of friction, φ_{mob}, as;

$$\eta = \frac{2\sin\phi_{mob}}{\sqrt{3}\left(3-\sin\phi_{mob}\right)} \tag{13}$$

The plastic potential is defined as;

$$\Psi = -\alpha' I_1 + \sqrt{J_2} - K = 0 \tag{14}$$

This plastic potential function, of the Drucker-Prager type, is similar to the yield function except that $g(\theta)$ in Eq. 11 is equal to unity. Eq. 14 is employed so as to have differentiability at all stress states. The factor α' depends on the type of analysis. The factor α' used in the present analysis under plane strain conditions is linked to the mobilized dilatancy angle ν as;

$$\alpha' = \frac{\tan\nu}{\sqrt{9+12\tan^2\nu}} \tag{15}$$

$$\nu = \arcsin\left(-\frac{d\varepsilon_1^{ir}+d\varepsilon_3^{ir}}{d\varepsilon_1^{ir}-d\varepsilon_3^{ir}}\right) \tag{16}$$

where $d\varepsilon_1^{ir}$ and $d\varepsilon_3^{ir}$ are the major and minor irreversible principal strain increments (positive in compression), which are linked to each other through the Rowe's stress-dilatancy relation (Rowe, 1962);

$$\frac{\sigma_1}{\sigma_3} = -K\left(\frac{d\varepsilon_1^{ir}}{d\varepsilon_3^{ir}}\right) \tag{17}$$

where K is a material constant (equal to 3.5 for Toyoura sand and 3.0 for Huston sand in the present case). As the model has the yield function and plastic potential surface having different forms, it is one of the non-normal plasticity models or non-associated flow models (Vermeer and de Borst, 1984).

5. FEM SIMULATION OF REINFORCING ELEMENTS

5.1 Problem definition

Fig. 2 shows the two generated nonlinear truss elements connected successively each other in the horizontal direction. At the left end of the two elements, a fixed hinge was given to the node. The tensile load was generated by a nodal velocity (or the tensile strain was generated by the nodal force) at the right end of the two elements. To simulate the load relaxation test during otherwise ML, the nodal velocity during that load relaxation stage is made zero. In addition, during the sustained loading, a point load must be given in addition to the one that has been generated by a given history of nodal velocity, which is set to be zero. By the above-mentioned procedures, the GNA will switch automatically between the displacement-controlled mode and the load-controlled mode.

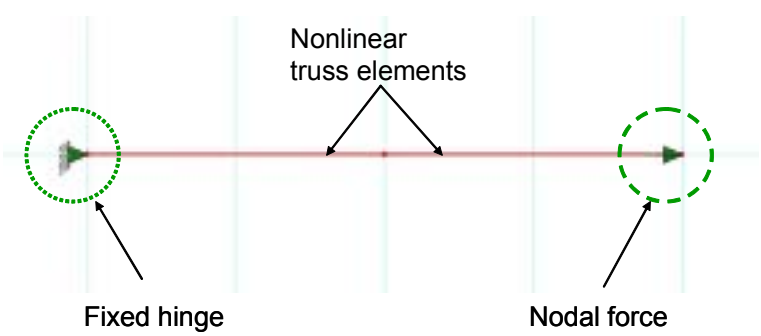

Figure 2 FEM nonlinear truss elements for the tensile loading test simulation

5.2 FEM simulation of tensile load-strain behaviour of geosynthetic reinforcement

Fig. 3 shows the two generated nonlinear truss elements connected successively each other in the horizontal direction. At the left end of the two elements, a fixed hinge was given to the node. The tensile load was generated by a nodal velocity (or the tensile strain was generated by the nodal force) at the right end of the two elements. To simulate the load relaxation test during otherwise ML, the nodal velocity during that load relaxation stage is made zero. In addition, during the sustained loading, a point load must be given in addition to the one that has been generated by a given history of nodal velocity, which is set to be zero. By the above-mentioned procedures, the GNA will switch automatically between the displacement-controlled mode and the load-controlled mode. It should be noted that, in the simulation of tensile loading test by FEM, the length of the connected truss elements does not affect the simulated results as long as the tensile strain rates are converted to the nodal velocities correctly. Neither of the number of nonlinear truss elements connected, the length of each element and the directions of element (i.e., horizontal or vertical) does affect the simulated results by FEM. Note also that, in the GNA, the nonlinear truss element is considered as a volumeless element. Consequently, only the stress and strain values of the nonlinear truss element are incorporated while its volumetric change is not considered.

Although many types of reinforcing materials have been simulated by FEM, only Polyester (PET) has been reported here as it is used in the PSC test simulation as well. Details of the other materials can be found elsewhere (Kongkitkul Warat (2004)). For PET, Vmax, nominal (kN/m)= 39.2 (is the value provided by the manufacturers) at strain rate 1 %/min.

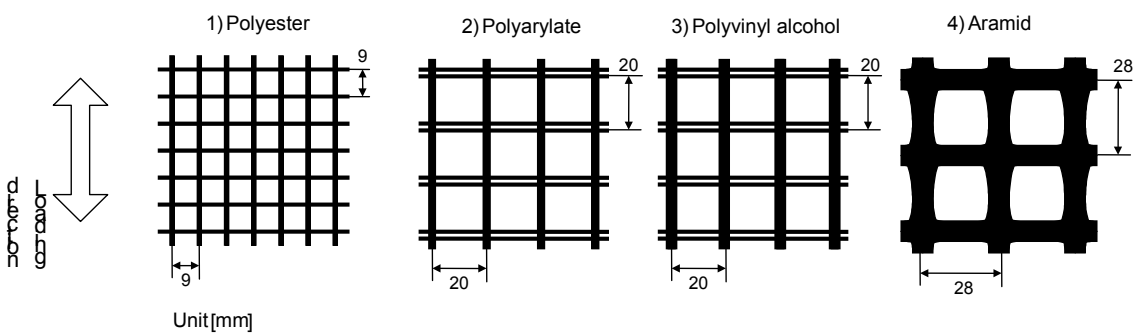

Figure 3 Different types of geosynthetic reinforcements.

5.3 Loading histories implemented in FEM simulations

From the various schemes of loading history employed to evaluate the viscous properties of the geosynthetic reinforcements, the following schemes of loading history were selected to be simulated by FEM:

a) The strain rate was changed stepwise several times and a set of sustained loading and load relaxation tests were performed during otherwise ML at a constant strain rate.
b) Sustained loading tests were performed during otherwise primary ML at a constant strain rate of 0.1 %/min.
c) Sustained loading tests were performed during otherwise primary ML at a constant strain rate of 1.0 %/min.

5.4 Elastic properties of geosynthetic reinforcements

By performing a small-amplitude cyclic loading tests during otherwise ML at a constant strain rate, the equivalent elastic stiffness, k_{eq}, as a function of tensile load, V,can be obtained. It is to be noted that the peak-to-peak secant modulus of respective unload/reload cycle was defined as k_{eq}. The value of k_{eq} is not constant with respect to load V, but it is a function of the instantaneous load, V. Elastic stiffness, k_{eq} (kN/m) of PET specimen was found to be 2000. These values are the average for a range of tensile load from zero to the rupture of the respective type of reinforcement.

5.5 Plastic properties of geosynthetic reinforcements

The relationship between the tensile load and the tensile strain of a given type of geosynthetic reinforcement usually exhibits a high non-linearity. In the GNA, any function can be used to fit the inviscid tensile load-irreversible strain ($V^f \sim \varepsilon^{ir}$) (i.e., reference relation). The following polynomial equation was employed to express the $V^f \sim \varepsilon^{ir}$ relationship:

$$V^f = \sum_{i=1}^{10} a_i \cdot \left(\varepsilon^{ir}\right)^{i-1} \tag{18}$$

where a_i is the coefficient (Eq. 19) for the term i, which was determined so that Eq.18 could best fit the respective inferred load-strain relationship in ML at zero strain rate that was extrapolated from the test results. In this inference, it was taken into account that the load and strain state ultimately reaches, at infinite time, the reference relationship in the case of the isotach viscosity.

$$\begin{aligned} &a_1 = 0; a_2 = 814.51; a_3 = -38186.49; a_4 = 1.01013\times10^6; \\ &a_5 = -1.45177\times10^7; a_6 = 1.15334\times10^8; a_7 = -4.69927\times10^8; a_8 = 7.66542\times10^8 \end{aligned} \tag{19}$$

5.6 Viscous properties of geosynthetic reinforcements

Eq. 20 lists parameters of the viscosity and decay functions in the non-linear three-component model used in FEM simulation for the respective geosynthetic reinforcement type.

$$\begin{aligned} &\lambda^v = 0.8; \\ &\alpha = 0.70; m = 0.12; \\ &r_i = 1.0; r_f = 0.15; c = 0.40; n = 0.6 \end{aligned} \tag{20}$$

5.7 Results of FEM simulation for geosynthetic reinforcements

Fig. 4 shows the result from the FEM analysis of reinforcement 1 (Polyester) subjected to loading history of stepwise changes in the strain rate, sustained loading and load relaxation, incorporating the three-component model with the combined type viscosity of the tensile test, compared with the experimental data. It may be seen that the whole details of the viscous behaviour of reinforcement 1 is well simulated by the FEM. Figs. 5 and 6 show, respectively, the time histories of tensile load and tensile strain obtained from the FEM analysis that correspond to the tensile load-strain relation presented in Fig. 4. It could be seen also that both time histories of tensile load and tensile strain are simulated very well by the FEM.

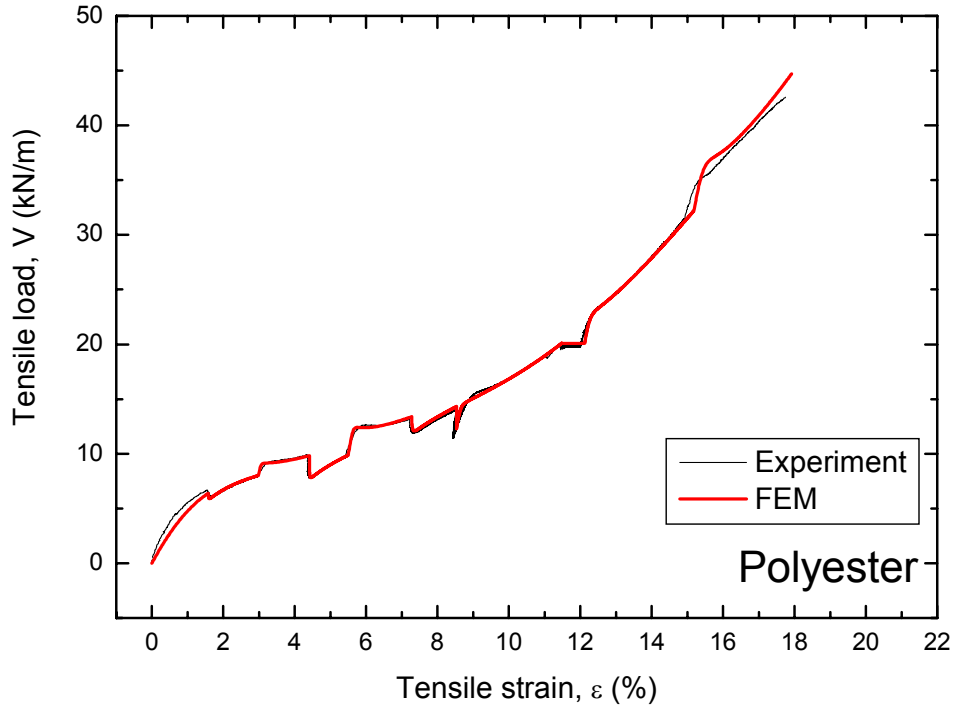

Figure 4 FEM simulation of tensile load-strain relation from stepwise changes in the strain rate, sustained loading and load relaxation tests, reinforcement 1 (Polyester)

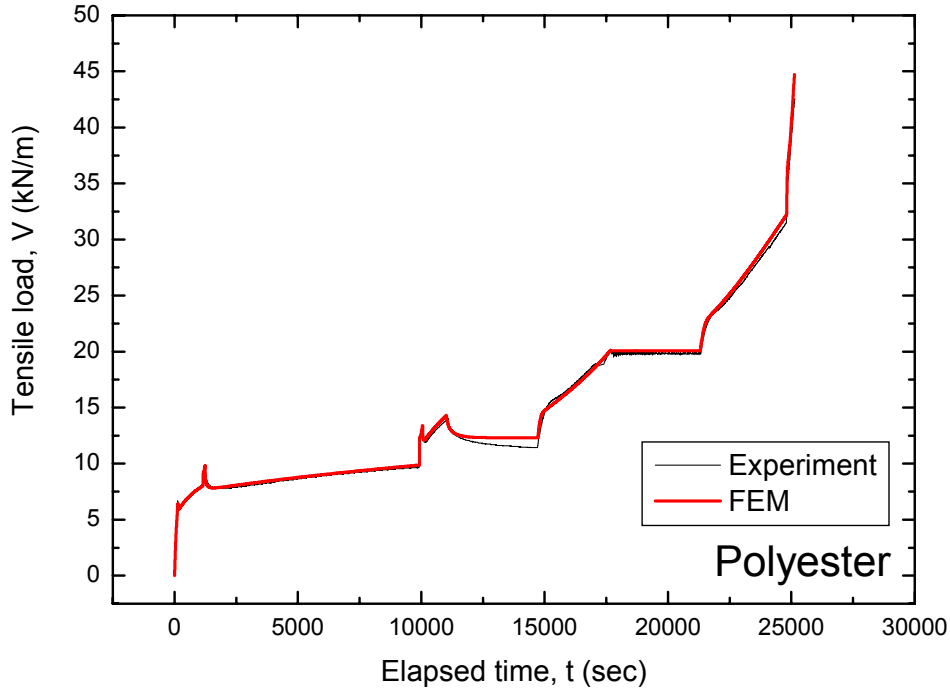

Figure 5 FEM simulation of time history of tensile load presented in Fig. 4, reinforcement 1 (Polyester)

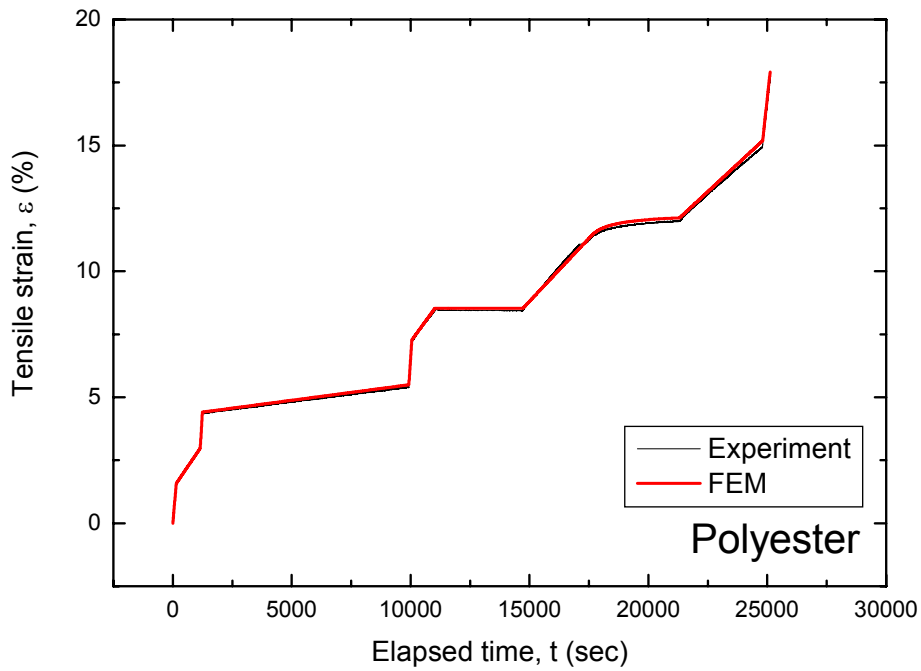

Figure 6 FEM simulation of time history of tensile strain presented in 4, reinforcement 1 (Polyester)

6. FEM SIMULATION OF PET GEOGRID-REINFORCED SAND IN PSC

After having finished the FEM analysis on the geosynthetic reinforcement alone, the FEM analysis of the PSC behaviour of reinforced sand was performed. In this section, first, the results from FEM analysis of PSC test on the PET geogrid-reinforced sand specimen (i.e., TEST008) are described. The mesh having 24 x 24 = 576 elements was firstly generated. Each element has initial dimensions of 4 mm-wide by 5 mm-high. The global initial width and height of specimen are 96 mm and 120 mm, respectively, that are the same as the dimensions

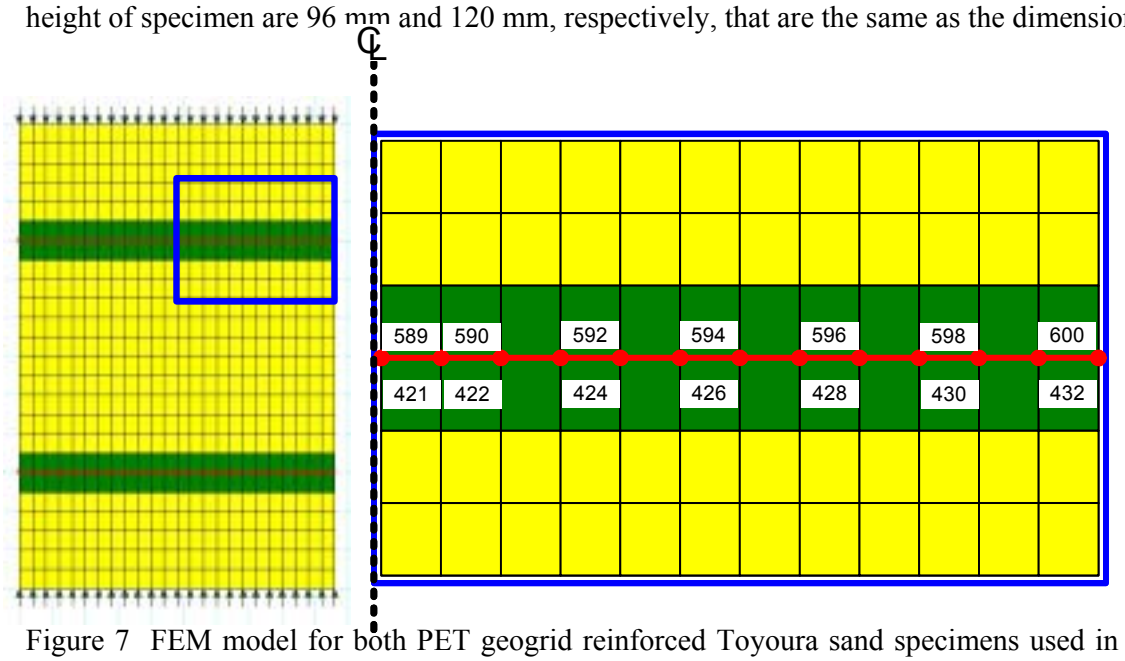

Figure 7 FEM model for both PET geogrid reinforced Toyoura sand specimens used in the present study

of specimen used in the experiment of reinforced sand specimen in PSC. In addition to the generated FEM mesh used in the simulation of unreinforced sand, two lines of connected nonlinear truss elements, which are representing the two layers of geogrid, were arranged at the one forth and the three forth of the height of specimen, respectively (Fig. 7). In the PSC test, he specimens were rectangular-prismatic of 20 cm high, 16 cm long and 8 cm wide (in the σ_3 direction) with well-lubricated top and bottom ends and σ_2 surfaces. The specimens were prepared by pluviating air-dried sand particles through air.

The average shear strength of sand in contact with a reinforcement layer having an aperture is lower than the value of sand in contact with a planar reinforcement layer without any opening under otherwise same conditions. The average shear strength along the interface increases with an increase in the covering ratio (CR) of the geogrid under otherwise the same conditions. Subsequently, the nodal velocities are equally applied (heading to each other) at the top and bottom boundaries of the FEM mesh. The values of nodal velocity were determined and then converted from the time history of vertical strain measured in the experiment. Then, an initial confining pressure of 30 kPa was applied to the FEM mesh before the start of the execution of PSC loading.

6.1 Global stress-strain relation of PET geogrid-reinforced sand

Fig. 8 shows the measured and simulated average stress-average strain relation R - ε_v relation from a drained PSC test on dry Toyoura sand (a Japanese sand with D_{50}= 0.18 mm, U_c= 1.64, G_s= 2.65, e_{max}= 0.99 and e_{min}= 0.62). It may be seen that the overall stress-strain behaviour is well simulated. Moreover, the simulated result exhibits noticeable trend of behaviour with stress jumps upon the stepwise changes in the strain rate, creep deformation at sustained loading and

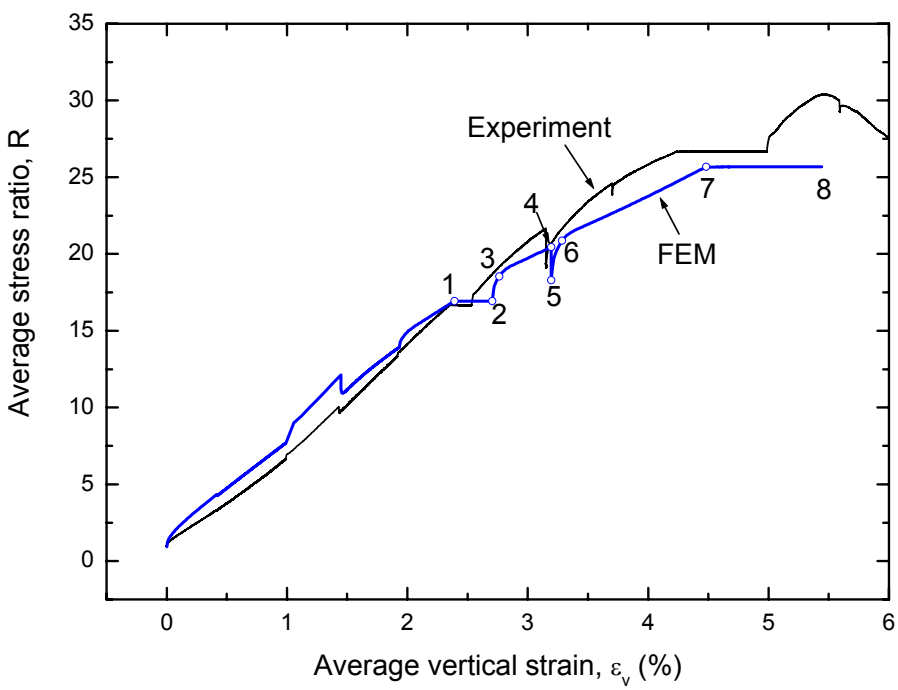

Figure 8 Simulation of the average stress ratio and average vertical strain relation of PET geogrid-reinforced sand, TEST008

stress relaxation that are similar to those observed in the experiment. Note that the numbers '1' to '8' are given on the average stress-average strain relation from the FEM for the subsequent discussions. The use of numbering instead of lettering is to distinguish the results from FEM and experiment.

6.2 Local tensile load-strain relations of PET geogrid

Figs. 9 and 10 show the local tensile load-tensile strain relations of geogrid elements 589 and 598 (see Fig. 7 for the locations of this geogrid element). The local behaviours of geogrid elements 589 and 598 adjacent to the centre and near the edge of specimen are selected for the discussions below. The following trends of behaviour may be seen from these two geogrid elements:

The trends of viscous behaviour of the geogrid are obvious.

1) The tensile force in element 589 (near the centre) is much larger than the one in element 598 (near the edge), which is a natural consequence of the fact that the shear stresses act in the outward direction along the boundary between the geogrid and the sand.

2) At stress relaxation stage '4'-'5', the tensile force in the geogrid decreases with time.

3) At the sustained loading stage '1'-'2', the tensile force in the geogrid decreases with time despite that the boundary stresses are kept constant. This trend of behaviour is the same as the one predicted by the direct numerical analysis of the PSC test result by the three-component model. This result indicates that the possibility of creep rupture of geogrid becomes very low even if sustained loading continues for a long duration.

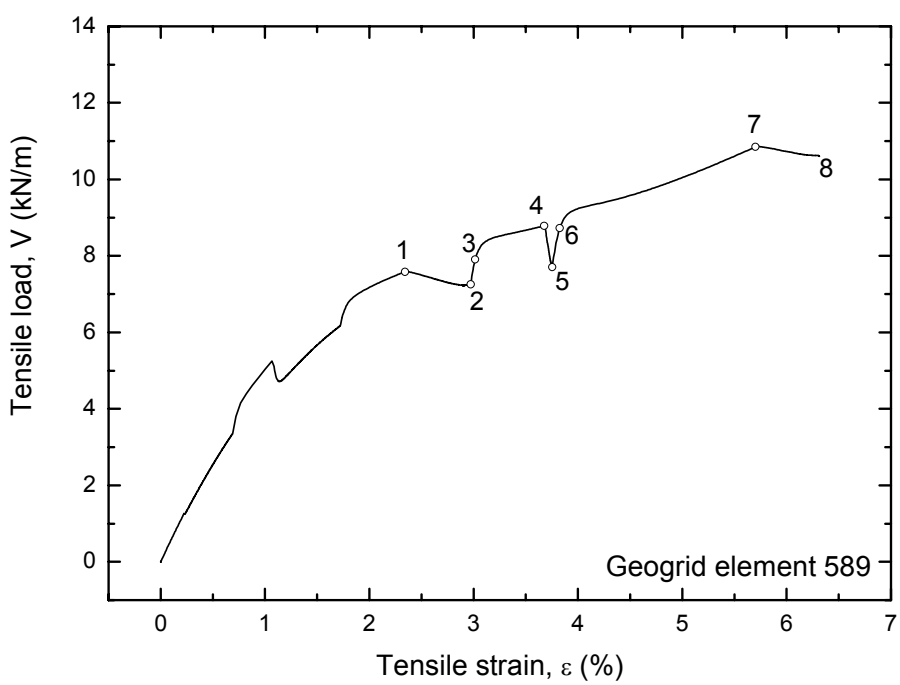

Figure 9 Local force and strain relation of PET geogrid in geogrid element 589, TEST008

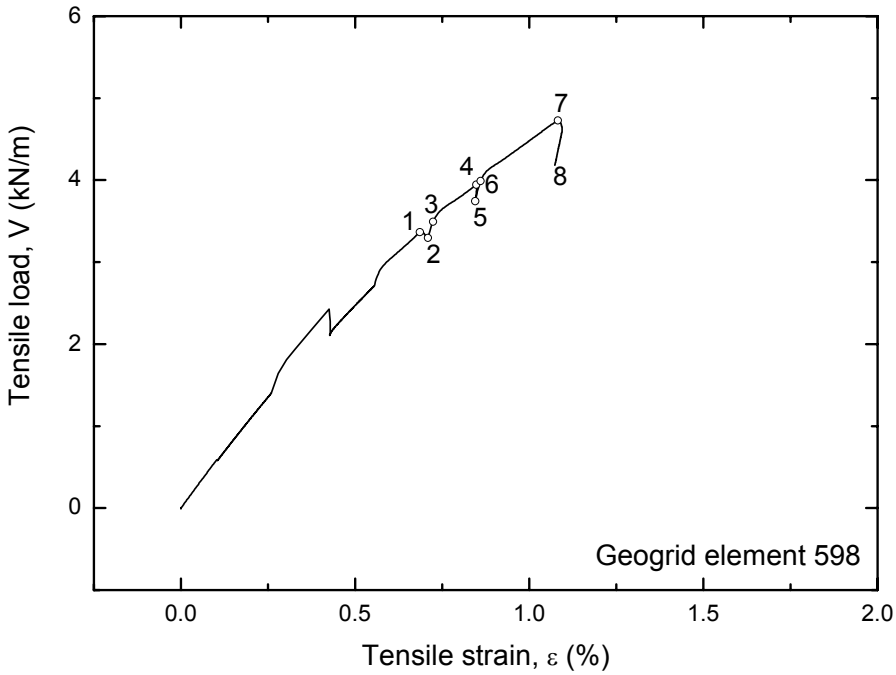

Figure 10 Local force and strain relation of PET geogrid in geogrid element 598, TEST008

7. CONCLUSING REMARKS

1) The FEM code incorporating the non-linear three-component model is able to realistically simulate the results from tensile tests on geosynthetic reinforcements alone, and PSC tests on sand alone and geosynthetic-reinforced sand.
2) Geosynthetic-reinforced sand exhibits a significant trend of viscous behaviour due to the viscous properties of not only geosynthetic but also sand. Consequently, any analysis of the residual deformation by sustained loading of a given GRS structure not taking into account the viscous properties of backfill or geosynthetic or both is not relevant. The current design procedure based on the creep rupture curve of geosynthetic only is therefore not relevant.

3) The FEM analysis of the geogrid-reinforced PSC test result incorporating the non-linear three-component model for the viscous properties of both sand and geogrid indicates that, due to an interaction between the viscous behaviours of geogrid and sand, the tensile force in the geogrid arranged in the sand specimen decreases with time during sustained loading at a constant load of specimen when the sustained load level is sufficient lower than the failure load. This is due to the effect of load relaxation of geosynthetic and compressive lateral creep by confining pressure provided by tensile reinforcing overtaking the effect of extending lateral creep associated with the compressive vertical creep by Poisson's effect. This result suggests that it could be too conservative to assume that the tensile force in the geogrid reinforcement arranged in the full-scale backfill is maintained constant during service at constant working load.

REFERENCES

Di Benedetto,H. (1987) Modélisation du comportement des géomatériaux: application aux enrobés bitumineux et aux bitumes, **Thèse de Docteur d'Etat ès Sciences, INPG-USTMG-ENTPE**, p.310 (in French).

Di Benedetto,H. and Tatsuoka,F. (1997) Small strain behaviour of geomaterials: modelling of strain effects, **Soils and Foundations**, Vol.37, No.2, pp.127-138.

Di Benedetto,H,, Sauzeat,C. and Geoffroy,H. (2001) Modelling viscous effects and behaviour in the small strain domains **Proc. 2nd Int. Symp. on Prefailure Deformation Characteristics of Geomaterials, IS Torino** (Jamiolkowski et al., eds.), Vol.2, pp.1357-1367.

Di Benedetto,H., Tatsuoka,F. and Ishihara,M. (2002) Time-dependent shear deformation characteristics of sand and their constitutive modeling **Soils and Foundations**, Vol. 42, No.2, pp.1-22.

Hirakawa,D., Ishihara,K., Tatsuoka,F. and Okajima,S. 1998. Some aspects of optimum geotextile design for reinforced sand considering aperture and stiffness of geotextile, **Proc. of the 33rd Japan National Conf. on Geotechnical Engineering, JGS (Yamaguchi)**, pp.2333-2334 (in Japanese).

Hoque,E. and Tatsuoka,F. (1998) Anisotropy in the elastic deformation of materials", Soils and Foundations **Soils and Foundations**, Vol.38, No.1, pp.163-179.

Kiyota, T., Tatsuoka,F. and Yamamuro,J. (2004) Drained and undrained creep characteristics of loose saturated sand and their relation, **GeoFrontier05**, GeoInstitute, Austin, Texas.

Kongkitkul Warat (2004), Effect of material viscous properties on the residual deformation of geosynthetic-reinforced sand, **Ph.D. Thesis**, Tokyo University.

Kotake,N., Tatsuoka,F., Tanaka,T., Siddiquee,M.S.A. and Yamauchi,H. 1999. An insight into the failure of reinforced sand in plane strain compression by FEM simulation, **Soils and Foundations**, Vol.39, No.5, pp.103-130.

Kuwano,R. and Jardine,R.J. (2002) On measuring creep behaviour in granular materials through triaxial testing, **Canadian Geotechnical Journal**, Vo.39, pp.1061-1074.

Lade,P. and Liu,C-t. (1998) Experimental study of drained creep behavior of sand, **Journal of Engineering Mechanics, ASCE**, 124-8, pp.912-920.

Matsushita,M., Tatsuoka,F., Koseki,J., Cazacliu,B., Di Benedetto,H. and Yasin,S.J.M. (1999) Time effects on the pre-peak deformation properties of sands, **Proc. Second Int. Conf. on Pre-Failure Deformation Characteristics of Geomaterials, IS Torino '99** (Jamiolkowski et al., eds.), Balkema, Vol.1, pp.681-689.

Nawir,H., Tatsuoka,F. and Kuwano,R. (2003) Viscous effects on the shear yielding characteristics of sand, **Soils and Foundations**, Vol.43, No.6, pp.33-50.

Ortiz, M. And Simo, J. C. (1986) An analysis of a new class of integration algorithms for elastoplastic constitutive relations, **International Journal for Numerical Methods in Engineering**, Vol. 23, pp.353-366.

Peng,F.L., Kotake,N., Tatsuoka,F., Hirakawa,D. and Tanaka,T. 2000. Plane strain compression behaviour of geogrid-reinforced sand and its numerical analysis, **Soils and Foundations**, Vol.40, No.3, pp.55-74.

Rowe, P. W., (1962) The Stress dilatancy relation for static equilibrium of an assembly of particles in contact, **Proceedings of Royal Society,** London, series A, pp. 500-527.

Siddiquee,M.S.A., Tanaka,T., Tatsuoka,F., Tani,K. and Morimoto,T. (1999), FEM simulation of scale effect in bearing capacity of strip footing on sand, **Soils and Foundations***,* Vol.39, No.4, pp.91-109.

Siddiquee, M. S. A., Tatsuoka, F., Tanaka, T. , Tani, K., Yoshida, K. and Morimoto, T. (2001a); Model tests and FEM simulation of some factors affecting the bearing capacity of footing on sand, **Soils and Foundations***,* Vol.41, No.2, pp.53-76.

Siddiquee, M. S. A. And Tatsuoka, F. (2001b), Modeling time-dependent stress-strain behaviour of stiff geomaterials and its applications, **Proc. 10th International Conference on Computer Methods and Advances in Geomechanics (IACMAG),** Tucson, Arizona on january 7-12.

Tatsuoka, F., Siddiquee, M. S. A., Park, C.-S., Sakamoto, M. and Abe, F., (1993) Modelling stress-strain relations of sand, **Soils and Foundations**, Vol. 33, No.2, pp. 60-81.

Tatsuoka,F. and Kohata,Y. (1995) Stiffness of hard soils and soft rocks in engineering applications, **Keynote Lecture, Proc. of Int. Symposium Pre-Failure Deformation of Geomaterials** (Shibuya et al., eds.), Balkema, Vol. 2, pp.947-1063.

Tatsuoka,F., Jardine,R.J., Lo Presti,D., Di Benedetto,H. and Kodaka,T. (1999) Characterising the Pre-Failure Deformation Properties of Geomaterials, Theme Lecture for the Plenary Session No.1, **Proc. of XIV IC on SMFE, Hamburg***,* September 1997, Volume 4, pp.2129-2164.

Tatsuoka,F., Santucci de Magistris,F., Hayano,K., Momoya,Y. and Koseki,J. (2000) Some new aspects of time effects on the stress-strain behaviour of stiff geomaterials, Keynote Lecture, **The Geotechnics of Hard Soils – Soft Rocks, Proc. of Second Int. Conf. on Hard Soils and Soft Rocks, Napoli, 1998** (Evamgelista and Picarelli eds.), Balkema,Vol.2.

Tatsuoka,F., Uchimura,T., Hayano,K., Di Benedetto,H., Koseki,J. and Siddiquee,M.S.A. (2001), Time-dependent deformation characteristics of stiff geomaterials in engineering practice, the Theme Lecture, **Proc. of the Second International Conference on Pre-failure Deformation Characteristics of Geomaterials, Torino, 1999, Balkema** (Jamiolkowski et al., eds.), Vol. 2, pp.1161-1262.

Tatsuoka,F., Ishihara,M., Di Benedetto,H. and Kuwano,R. (2002) Time-dependent shear deformation characteristics of geomaterials and their simulation, **Soils and Foundations**, Vol. 42, No.2, pp.103-129.

Vermeer, P. A. and de Borst, R. (1984) Non-associated plasticity for soils, concrete and rock, **Heron**, **29(3)**, 1-64.

Villard,P., Kotake,N. and Otani,J. 2002. Modelling of reinforced soil in finite element analysis, Keynote Lecture, **Proc. of the 7th International Conference on Geosynthetics**, Nice, Vol.1, pp.35-95.